

Audio-Visual World Models: Towards Multisensory Imagination in Sight and Sound

Jiahua Wang^{1,*}, Leqi Zheng^{1,*}, Jialong Wu¹, and Yaoxin Mao²

¹ Tsinghua University

² Beijing Institute of Technology

*Equal contribution

Abstract. World models simulate environmental dynamics to enable agents to plan and reason about future states. While existing approaches have primarily focused on visual observations, real-world perception inherently involves multiple sensory modalities. Audio provides crucial spatial and temporal cues such as sound source localization and acoustic scene properties, yet its integration into world models remains largely unexplored. No prior work has formally defined what constitutes an audio-visual world model or how to jointly capture binaural spatial audio and visual dynamics under precise action control. This work presents the first formal framework for Audio-Visual World Models (AVWM), formulating multimodal environment simulation as a partially observable Markov decision process with synchronized audio-visual observations. To address the lack of suitable training data, we construct AVW-4k, a dataset comprising 30 hours of binaural audio-visual trajectories with action annotations across 76 indoor environments. We propose AV-CDiT, an **A**udio-**V**isual **C**onditional **D**iffusion **T**ransformer with a novel modality expert architecture that balances visual and auditory learning, optimized through a three-stage training strategy for effective multimodal integration. Extensive experiments demonstrate that AV-CDiT achieves high-fidelity multimodal prediction across visual and auditory modalities. Furthermore, we validate its practical utility in continuous audio-visual navigation tasks, where AVWM significantly enhances the agent’s performance.

Keywords: World Model · Multimodal · Diffusion Transformer

1 Introduction

In recent years, large-scale pre-trained models have significantly advanced a wide range of AI applications. A natural extension of this success is to equip models with the ability to predict and reason about future states of the world. In this context, world models [12, 19, 21, 51, 54] have emerged as a fundamental paradigm for enabling AI systems to understand and simulate environmental dynamics. World models aim to encode the underlying dynamics of an environment, allowing an agent to predict future observations based on its actions,

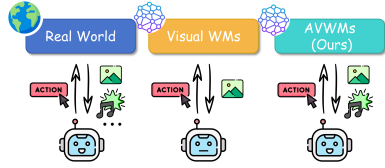


Fig. 1: From unimodal to audio-visual world models. Our work introduces AVWMs to jointly simulate synchronized audio-visual dynamics.

Table 1: Comparison with existing world modeling approaches.

Method	Modality	Precise Action	Binaural Audio
DIAMOND [2]	Visual	✓	✗
Genie [6]	Visual	✗	✗
Cosmos [1]	Visual	✗	✗
VLWM [49]	Visual+Text	✗	✗
RLVR-World [43]	Visual+Text	✓	✗
AV-CDiT	Visual+Audio	✓	✓

thereby providing a foundation for planning, decision making, and reasoning in complex environments. While early world modeling efforts predominantly focused on visual observations, real-world perception is inherently multimodal. Among the various sensory modalities, audio carries rich information about environmental properties that are often complementary to visual cues [13,38,52,53]. For instance, the spatial location of sound sources, the acoustic characteristics of physical spaces, and the temporal evolution of auditory events all provide critical signals for embodied agents navigating and interacting with their surroundings. As such, developing world models that can jointly capture audio-visual dynamics under precise action control represents an essential step toward building intelligent agents capable of human-like environmental understanding.

However, existing research faces two major limitations that hinder progress toward multimodal world modeling.

Limitation 1: Conceptual and data-level gap in constructing audio-visual world models. Although multimodal perception has become a central goal for embodied intelligence, there remains no formalized definition of what constitutes an audio-visual world model. Prior work has not clarified how synchronized audio observations, visual observations and fine-grained actions should be jointly modeled within a unified world-dynamics formulation. There is also a lack of standardized datasets. Existing datasets are either purely visual or provide entire audio and video tracks that lack action-conditioned correspondence. Besides they hardly capture spatial acoustic characteristics, making them unsuitable for constructing and evaluating controllable audio-visual world models.

Limitation 2: Architectural gap in modeling controllable multimodal dynamics. Even if such a formulation were available, current modeling paradigms remain inadequate for learning coherent and controllable multimodal world dynamics. As summarized in Table 1, existing world models mostly focus solely on visual dynamics. Although some multimodal world model architectures extend beyond vision to incorporate modalities such as text, they are primarily designed to capture semantic associations rather than temporally aligned sensory dynamics. Moreover, these models do not facilitate the simultaneous generation of multiple modalities. Consequently, these architectures remain inadequate for audio-visual world modeling, where the audio modality is inherently synchronized with visual signals over time.

As illustrated in Figure 1, while real-world embodied agents naturally perceive through both visual and auditory channels, existing world models remain confined to unimodal visual prediction. This raises a critical question: *How can we formally define and implement an audio-visual world model that accurately captures synchronized multimodal dynamics under precise action control while predicting environmental feedback?*

To bridge these gaps, we re-examine world modeling from a multimodal perspective, arguing that a genuine world model must capture how actions propagate through both the visual and acoustic domains over time. Our contributions are threefold:

- **Formal Problem Formulation and Dataset:** To address the first limitation, we provide the first formal definition of Audio-Visual World Models (AVWM), establishing a unified framework for modeling binaural spatial audio, visual observations and precise action control within a POMDP formulation. To support this formulation, we construct AVW-4k, comprising approximately 30 hours of synchronized binaural audio-visual data with action annotations across 76 indoor environments (Section 3).
- **Modality Expert with Stagewise Training:** To address the second limitation, we design AV-CDiT, an Audio-Visual Conditional Diffusion Transformer featuring a novel modality expert architecture that balances cross-modal interaction while preserving modality-specific representations. We further develop a three-stage training strategy that ensures stable optimization and enhances multimodal integration (Section 4).
- **Comprehensive Experimental Validation:** We conduct extensive experiments demonstrating that our model achieves high-fidelity multimodal prediction across visual and auditory modalities, and serves as an effective planning tool for continuous audio-visual navigation tasks, validating its utility for downstream embodied AI applications (Section 5).

2 Related Works

Multimodal World Models. World models aim to simulate environment dynamics through internalized commonsense knowledge [42]. While unimodal models like DIAMOND [2], Genie [6] and Cosmos [1] achieve high-fidelity visual prediction, they lack **the multi-sensory feedback** essential for real-world intelligence. Recent studies [44] suggest that modalities provide complementary reasoning pathways: text offers semantic abstractions, while visual generation grounds spatial and physical intuition. We argue that audio adds an indispensable dimension, capturing temporal dynamics and non-line-of-sight interactions often ambiguous in other modalities. Furthermore, current world models rarely support **simultaneous multimodal generation**. As shown in Table 1, while advanced frameworks like VLWM [49] and RLVR-World [43] incorporate multiple modalities, they do not generate paired, synchronized outputs. Our work enables joint, synchronous generation of visual and auditory streams to capture

their intrinsic physical links. This coupled simulation provides a fertile research ground for exploring cross-modal alignment within world models.

Audio-visual Generation. Audio-visual generation tasks encompass cross modal generation (e.g., audio to video), multimodal interpolation, and audio-visual continuation [27]. The latter two tasks generally provide a temporally aligned audio-visual segment as conditioning and require the model to predict or fill in a specified portion of audio and video, ensuring that the entire sequence remains temporally coherent. Recent works [37, 39, 45] have proposed versatile audio-visual models, but they typically generate content conditioned only on historical frames. Even works like WorldGPT [16], which frame themselves as world models, remain confined to vague language commands and lack explicit, fine-grained physical control. Consequently, these models function as conditional generators rather than true world models capable of counterfactual reasoning—answering "What if a different action were taken?" instead of merely "What happens next?". Nonetheless, they provide valuable insights for the audio-visual world model proposed in this work.

3 Formulation and Dataset

3.1 Audio-Visual World Models

An Audio-Visual World Model (AVWM) is designed to simulate an external environment containing sound signals. In this environment there exists a stationary sound source. We model this environment as a partially observable Markov decision process (POMDP), defined as a tuple $(\mathcal{S}, \mathcal{O}, \mathcal{A}, p, r)$. At each time step t , $s_t \in \mathcal{S}$ represents the underlying state of the environment. $o_t = \phi(s_t) = \{o_t^v, o_t^a\} \in \mathcal{O}$ represents the partial observation received by the agent, only providing incomplete information of s_t . $o_t^v \in \mathbb{R}^{H \times W \times 3}$ is the visual observation (an image frame) and $o_t^a \in \mathbb{R}^{L \times 2}$ is the binaural auditory observation (a short segment of binaural audio). Action $a_t = (u_t, \omega_t) \in \mathcal{A}$ specifies a spatial transformation of the agent, where u_i and ω_i denote the positional and orientational transformations, respectively.

Note that all actions in the discrete action space \mathcal{A} are executed with the same time duration. When a_t is executed at time step t , the environment transitions according to $p(s_{t+1} | s_t, a_t)$, yielding new audio-visual observations and, depending on the specific downstream task, an optional immediate reward $r_{t+1} = r(s_t, a_t)$. In our formulation, this task-specific reward serves as environmental feedback that reflects task progress, bridging the gap between raw perceptual changes and high-level task outcomes.

In order to simulate the the aforementioned environment, we describe an AVWM as follows:

$$\hat{o}_{t+\Delta t}, \hat{r}_{t+\Delta t} \sim p_{\theta}(o_{t+\Delta t}, r_{t+\Delta t} | o_{t-m+1:t}, a_{t \rightarrow t+\Delta t}, \Delta t), \quad (1)$$

where $o_{t-m+1:t}$ denotes the current observation along with its preceding frames, collectively referred to as the m -frame context. $a_{t \rightarrow t+\Delta t}$ denotes the spatial vector sum of the action sequence $a_{t:t+\Delta t}$ from the current frame o_t to the target

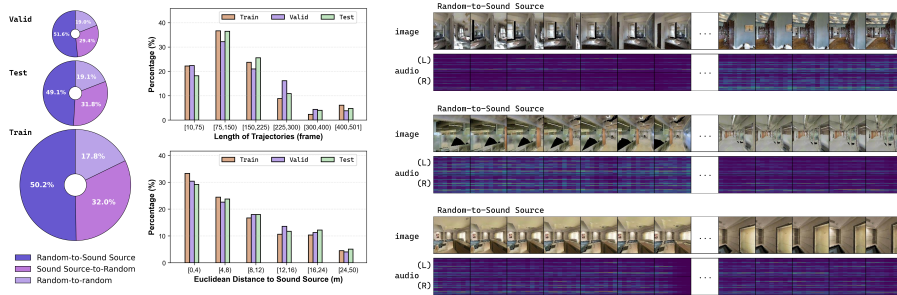


Fig. 2: Dataset statistics and trajectory examples of the proposed AVW-4k. **Left:** Proportions of trajectories corresponding to the three motion patterns in the train/validation/test splits. **Middle:** Distributions of trajectory lengths and geodesic distances to the sound source across all frames in the dataset. **Right:** Representative trajectories for each motion pattern, with audios shown as binaural spectrograms.

frame $o_{t+\Delta t}$. $\Delta t \in [T_{\min}, T_{\max}]$ specifies the temporal offset measured in frames, and reward $r_{t+\Delta t}$ is treated as an auxiliary output which is active only when downstream task objectives are defined.

The idea of conducting skip-step prediction by varying the temporal offset Δt follows [4], allowing the model not only to perform next-frame prediction. Such temporal abstraction enables the world model to learn how the environment evolves over different time horizons, thereby improving its understanding of long-term spatio-temporal dependencies and underlying physical dynamics.

3.2 AVW-4k Dataset

To train and evaluate our model, we construct AVW-4k, an audio-visual interaction dataset collected in simulated indoor environments.

Data Collection. Data collection is conducted within the simulation environment built upon the Matterport3D dataset [7] and the SoundSpaces 2.0 simulator [9]. This allows for physically accurate sound propagation with frequency-dependent acoustic effects such as reflection, absorption, and reverberation.

During data collection, an agent continuously moves within the simulated 3D scenes while recording synchronized auditory and visual observations at each timestep. Each environment contains a stationary sound source fixed at a known location, which continuously plays a looping telephone ringtone. The agent’s trajectories are randomly sampled according to three motion patterns: (1) moving from the source to a random goal position, (2) moving from a random start position toward the source, and (3) moving between two random positions independent of the source. All trajectories are ensured to be navigable and maintain a reasonable distance from the source to prevent silent recordings.

Each frame consists of an egocentric RGB image with a resolution of 128×128 pixels and a 0.15-second binaural audio segment sampled at 16 kHz, strictly time-aligned across modalities. The action space of AVW-4k include four actions: move

forward by 0.15 m, turn left by 10° , turn right by 10° and stop. Each sample contains no more than 500 frames.

Dataset Composition. The final AVW-4k dataset contains approximately 30 hours of audio-visual data, spanning 76 indoor scenes and 4,500 trajectories. Trajectory lengths vary depending on navigation paths and acoustic configurations. The dataset is divided into training, validation, and test splits with a ratio of 6 : 1 : 2, where the environments across subsets are non-overlapping, ensuring a fair evaluation of the model’s cross-scene generalization ability.

3.3 Comparison with Analogous Datasets/Benchmarks

To provide a **clear context for our choice of AVW-4k**, we compare it with several analogous datasets in Table 2, with detailed descriptions of each dataset provided immediately following the table. The evaluation dimensions used in our comparison are explained as follows:

- **Vision (Vis.) & Audio (Aud.):** Indicates whether the dataset contains synchronized visual and auditory streams.
- **Real/Syn.:** Distinguishes between real-world captured data (Real) and synthetic data (Syn.).
- **AV-Consistency:** Defined as the physical alignment between audio and video. If the audio contains components inconsistent with the visual content (e.g., voiceovers, commentary, or background music), it is considered inconsistent.
- **Action Type:** Categorized into **None**, **Text Prompt** (e.g., abstract descriptions like “washing dishes”), and **Precise Action** (e.g., low-level continuous actions like displacement and rotation).
- **For AVWM:** Provides an overall assessment of whether the dataset can support action-contingent audio-visual future prediction.

Dataset Descriptions.

AudioSet is a large-scale audio event dataset curated by Google researchers through manual annotation of 10-second YouTube segments. Primarily designed for passive recognition, it is unsuitable for AVWM because its audio often contains post-production dubbing or irrelevant noise (lacking physical AV-consistency) and it lacks low-level action labels required for action-contingent modeling.

Landscape dataset is a high-resolution collection of natural scenes, totaling approximately 26 hours. While it offers superior physical AV-consistency by accurately capturing environmental acoustics, it is a passive observation dataset that lacks any action labels.

EPIC-KITCHENS is a large-scale egocentric video dataset featuring 55 hours of unscripted daily activities in kitchens. It provides textual annotations of action segments (e.g., ‘*Stir chicken.*’) and object bounding boxes based on participants’ post-recording narrations, but without precise low-level actions.

Ego4D-Sounds consists of 1.2 million curated clips from Ego4D [18] and EPIC-KITCHENS, specifically designed to strengthen the correspondence between

Table 2: Comparison of AVW-4k with analogous datasets.

Dataset	Vis.	Aud.	AV-Cons.	Real/Syn.	Action Type	For AVWM
AudioSet [17]	✓	✓	✗	Real	None	✗
Landscape [28]	✓	✓	✓	Real	None	✗
EPIC-KITCHENS [10]	✓	✓	✓	Real	Text Prompt	✗
Ego4D-Sounds [8]	✓	✓	✓	Real	Text Prompt	✗
SCAND [25]	✓	✗	N/A	Real	Precise Action	✗
RoboNet [11]	✓	✗	N/A	Real	Precise Action	✗
Meta-World [47]	✓	✗	N/A	Syn.	Precise Action	✗
CSGO [33]	✓	✗	N/A	Syn.	Precise Action	✗
MineRL [20]	✓	✗	N/A	Syn.	Precise Action	✗
PLAICraft [22]	✓	✓	✗	Syn.	Precise Action	✗
AVW-4k (Ours)	✓	✓	✓	Syn.	Precise Action	✓

foreground actions and audio by disentangling ambient background sounds. However, the action data remains limited to post-annotated textual descriptions of activities, lacking the precise, low-level motion control.

SCAND is a large-scale, first-person-view dataset for socially compliant navigation, featuring 25 miles of human tele-operated driving demonstrations across indoor and outdoor environments using robots. While it provides precise low-level action data, including joystick commands and odometry, the dataset lacks synchronized audio streams, making it unsuitable for training AVWM.

RoboNet is a large-scale multi-robot interaction dataset featuring 162,000 trajectories and 15 million video frames. The dataset focuses on predicting future video frames conditioned on precise action sequences. While it is a pioneering work for real-world action-conditioned visual prediction, the total absence of the auditory modality makes it unsuitable for AVWMs.

Meta-World is an open-source simulated benchmark for robotic manipulation based on a simulated Sawyer arm. The environment provides only visual observations and robotic actions, with a total absence of audio signals.

CSGO dataset is derived from the modern FPS game Counter-Strike: Global Offensive, featuring 95 hours of human gameplay demonstrations scraped from public servers. While it provides precise action labels (high-frequency keyboard and mouse control vectors) aligned with visual game frames, the dataset does not contain any synchronized audio streams.

MineRL is a large-scale synthetic dataset based on Minecraft, featuring over 60 million state-action pairs generated from human demonstrations. While it holds significant research value for action-contingent behavior learning, its focus is primarily on visual pixels and game states without synchronized audio streams, making it unsuitable for AVWMs.

PLAICraft is a large-scale, multiplayer Minecraft interaction dataset featuring video, audio, and precise action sequences. Although it records low-level control data, its audio stream is contaminated by inseparable, mixed-in player micro-

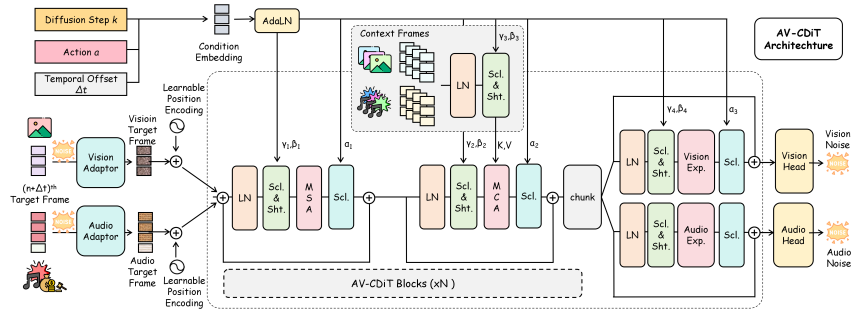


Fig. 3: Overview of the proposed AV-CDiT architecture.

phone speech. This mixing of environmental acoustics with external dialogue on a single track introduces significant components that are physically ungrounded in the visual stream. Consequently, it lacks the strict AV-consistency required for AVWMs.

4 Methodology

To implement the aforementioned AVWM, we design an integrated framework with two key innovations: the Audio-Visual Conditional Diffusion Transformer (AV-CDiT) featuring a novel modality expert architecture (Section 4.1), and a stagewise training strategy (Section 4.2).

4.1 Audio-Visual Conditional Diffusion Transformer

Model Architecture. AV-CDiT is a temporally autoregressive Transformer model capable of generating both visual and auditory frames. Building upon prior advances such as CDiT [4], which was originally developed for unimodal visual world models, AV-CDiT extends the diffusion framework to support action-conditioned multimodal generation through a novel architecture, illustrated in Figure 3.

AV-CDiT first employs two pre-trained and frozen encoders to encode visual frames o^v and auditory segments o^a , obtaining their respective latent representations z^v and z^a , similar in spirit to latent diffusion models [35].

Subsequently, latent representations from both modalities are projected into a shared latent space through separate adaptor layers for alignment. The scalar task reward $r_{t+\Delta t}$ is then broadcast to match the token dimensionality as a reward token $h_{t+\Delta t}^r$. Finally, the visual, auditory, and reward tokens are concatenated to form the target sequence, which is noised during diffusion.

$$X_{t+\Delta t} = [h_{t+\Delta t}^v : h_{t+\Delta t}^a : h_{t+\Delta t}^r]. \quad (2)$$

This target sequence is subsequently fed into a stack of AV-CDiT blocks for multimodal diffusion-based generation.

Similar to the target sequence, the context sequence is constructed by concatenating context frames from both visual and auditory modalities.

$$C_{t-m+1:t} = [[h_{t-m+1}^v : h_{t-m+1}^a], \dots, [h_t^v : h_t^a]]. \quad (3)$$

The conditioning embedding is generated following the CDiT formulation. The aggregated action $a_{t \rightarrow t+\Delta t}$, temporal offset Δt , and diffusion timestep k are encoded via sinusoidal features and two-layer MLPs to obtain ψ_a , $\psi_{\Delta t}$, and ψ_k , which are summed into a single conditioning vector c_t . This vector is then injected through an AdaLN [46] module to produce scale and shift parameters that modulate Layer Normalization and attention outputs, enabling conditional control during diffusion.

In each AV-CDiT Block, both visual and auditory tokens share common multi-head self-attention and cross-attention layers to enable joint modeling within a unified attention space. The self-attention layer facilitates cross-modal temporal coherence and semantic alignment, while the cross-attention layer conditions the fused target tokens on the context representations $C_{t-m+1:t}$, allowing each modality to exploit complementary information during generation.

Modality Experts. Inspired by previous expert network architectures [3, 41], each AV-CDiT block incorporates modality experts in the feed-forward layer that assign independent nonlinear mappings to each modality. After shared self-attention and cross-attention operations, the target sequence is divided into visual and auditory groups processed by corresponding modality expert sub-networks, with the reward token associated with the auditory branch, and outputs concatenated to reconstruct the unified sequence. This design prevents visual dominance from hindering auditory representation learning when leveraging visually pretrained models, enabling the auditory pathway to learn in a coordinated manner alongside the visual modality, which works in conjunction with the stagewise training strategy in Section 4.2 and is validated in Section 5.4. After multiple stacked blocks, visual, auditory, and reward tokens are decoded through respective output heads to predict noise, with denoised tokens decoded into future observations and the reward token average-pooled to estimate future task reward.

Diffusion Training. We follow the DDPM [24] formulation to model future multimodal generation as a synchronized diffusion process across both visual and auditory-reward modalities. Given the clean latent targets $X_{t+\Delta t}^v$ and $X_{t+\Delta t}^{a:r}$, Gaussian noise is independently injected into each modality according to a shared noise schedule $\{\bar{\alpha}_k\}_{k=1}^K$, while preserving their intrinsic correlation in the clean space:

$$\begin{aligned} X_{t+\Delta t}^{v,(k)} &= \sqrt{\bar{\alpha}_k} X_{t+\Delta t}^v + \sqrt{1 - \bar{\alpha}_k} \epsilon_v, \\ X_{t+\Delta t}^{a:r,(k)} &= \sqrt{\bar{\alpha}_k} X_{t+\Delta t}^{a:r} + \sqrt{1 - \bar{\alpha}_k} \epsilon_{a:r}, \end{aligned} \quad (4)$$

where $\epsilon_v, \epsilon_{a:r} \sim \mathcal{N}(0, I)$ are modality-specific Gaussian noises.

This formulation assumes conditionally independent forward noising processes for the two modalities. Meanwhile, the multimodal dependency is retained in the reverse process through a unified denoising network.

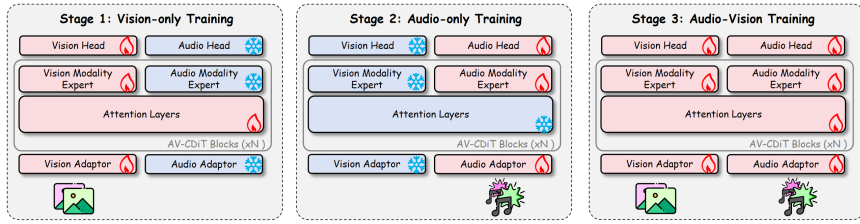


Fig. 4: Illustration of the stagewise training strategy used for AV-CDiT.

The reverse process is parameterized by AV-CDiT, which jointly predicts the injected noises ($\hat{\epsilon}_v, \hat{\epsilon}_{a:r}$) in a single forward pass.

Training Objective. AV-CDiT adopts the standard ϵ -prediction objective, estimating the noise added at each step rather than directly reconstructing clean targets. The loss is defined as:

$$\mathcal{L}_{\text{simple}} = \mathbb{E}_{k, \epsilon_v, \epsilon_{a:r}} [\|\hat{\epsilon}_v - \epsilon_v\|_2^2 + \|\hat{\epsilon}_{a:r} - \epsilon_{a:r}\|_2^2]. \quad (5)$$

Following [34], we predict the covariance matrix of the noise and supervise it with the variational lower-bound loss \mathcal{L}_{vb} [32], yielding the final objective $\mathcal{L} = \mathcal{L}_{\text{simple}} + \lambda_{\text{vb}}\mathcal{L}_{\text{vb}}$.

4.2 Stagewise Training Strategy

Inspired by previous work on multimodal joint pre-trainings [3, 41], we adopt a three-stage training strategy to ensure stable optimization and efficient convergence of the multimodal diffusion model, illustrated in Figure 4.

In the first stage, the model is trained on vision-only data to learn spatial-temporal representations by jointly optimizing the self-attention layers, cross-attention layers, visual modality experts, visual adaptor layer, and visual head. In the second stage, only the auditory modality experts, auditory adaptor layer, and auditory head are fine-tuned on audio-only data while freezing all other components, including shared attention modules and vision-related layers, to preserve previously acquired visual capabilities and prevent strong visual priors from suppressing auditory representation learning. The reward token is incorporated into the auditory sequence to enable joint modeling of auditory patterns and their associated rewards. In the third stage, visual and auditory inputs are concatenated and the entire network undergoes end-to-end fine-tuning on synchronized audio-visual data, allowing all parameters to be jointly optimized for deeper multimodal fusion and improved consistency across generated visual frames, audio segments, and predicted rewards within the unified temporal diffusion process.

5 Experiments and Results

5.1 Experimental Setting

Evaluation Metrics. For the image results, following prior works on unimodal visual world models [4, 43], we apply LPIPS [50] and DreamSim [15] to measure

perceptual similarity between predicted and ground-truth frames based on deep visual features, PSNR for pixel-level quality, and Fréchet Inception Distance (FID) [23] to evaluate the generated data distribution.

For the audio results, since the AVWM formulation requires a much higher degree of temporal and perceptual consistency between the generated and ground-truth audio than typical audio-visual generation tasks [27,37], we adopt not only Fréchet Audio Distance (FAD) [26] to assess overall audio realism, but also several fine-grained metrics commonly used in audio-related generation tasks such as speech restoration [31], and audio super-resolution [29]. Specifically, we compute Log-Spectral Distance (LSD) [14] to evaluate frequency-domain deviation and Spectral Structural Similarity (SSIM) [40] to measure structural coherence between predicted and reference spectrograms. Since our model generates binaural audio, all audio metrics are computed independently on each channel and then averaged. Additionally, for FAD evaluation, both the generated and ground-truth audio signals are zero-padded to ensure compatibility with the VGGish model used for feature extraction.

For the reward prediction results, we directly employ the Mean Squared Error (MSE) as the evaluation metric.

Encoder Configuration. For the visual encoder, we use the Stable Diffusion [5] VAE tokenizer, similar to that employed in DiT [34] and CDiT. For the auditory encoder, we trained a SoundStream [48] tokenizer on AVW-4k, similar to that employed in AVDiT [27]. Notably, we remove one extraction block from the original SoundStream encoder-decoder architecture to better accommodate the shorter audio segments in our dataset.

Training Details. For the implementation of the stagewise training strategy, we first fine-tune a pretrained NWM model [4] of base size on the visual subset of the AVW-4k dataset. The model has been pre-trained on large-scale visual datasets and thus possesses certain visual reasoning capabilities. The parameters of its CDiT blocks, including those of the self-attention, cross-attention, and feed-forward layers, are then used to initialize the corresponding layers of an AV-CDiT model of identical size, marking the completion of the first stage of the stagewise training. Subsequently, we continue fine-tuning the model through the remaining two stages to complete the full stagewise training process.

The AV-CDiT model is trained with a context length of 4 frames. During training, each sample randomly selects 4 different navigation goals within a temporal window of ± 16 frames around the current timestep for prediction, following the training paradigm of CDiT.

We use the AdamW optimizer for training. The learning rates are set to 1.6×10^{-4} , 8×10^{-4} , and 1.6×10^{-4} for the three stages of training. The total batch sizes for the three stages are 512, 768, and 128, respectively. All experiments are conducted on a single machine equipped with eight NVIDIA A100 GPUs.

5.2 Comparison with Baselines

Setup. Since no existing world models are currently capable of synchronized audio-visual future prediction, we establish a series of modality-factorized base-

Table 3: Comparison with baselines. We report the mean and standard deviation for each metric calculated over three runs.

Models	Vision				Audio		
	LPIPS↓	DreamSim↓	PSNR↑	FID↓	LSD↓	SSIM↑	FAD↓
DIAMOND [2] + AudioLDM [30]	0.626 ± 0.000	0.447 ± 0.000	13.849 ± 0.002	52.852 ± 0.137	2.593 ± 0.001	0.485 ± 0.000	2.015 ± 0.004
NWM [4] + AudioLDM	0.382 ± 0.000	0.258 ± 0.000	16.539 ± 0.001	25.906 ± 0.034			
AV-CDiT (ours)	0.382 ± 0.000	0.255 ± 0.000	16.504 ± 0.005	24.347 ± 0.023	1.311 ± 0.000	0.547 ± 0.000	2.391 ± 0.001

lines. We first utilize state-of-the-art visual world models to demonstrate our competitive performance within the visual modality. For auditory generation, we augment these unimodal world models with a separate, state-of-the-art audio generator. These models collectively serve as counterparts to our approach.

- **DIAMOND** [2] is a visual-only diffusion-based world model built upon the UNet [36] architecture. Following the official implementation, we adopt DIAMOND in an offline reinforcement learning setting and train it on the AVW-4k dataset. The model performs autoregressive state prediction at an initial 32×32 resolution, which is subsequently processed by an upsampler to reach the final 128×128 output. A linear embedding layer is employed to accommodate continuous action spaces.
- **NWM** [4] is a visual-only world model based on the Conditional Diffusion Transformer (CDiT) architecture. Following its official implementation, we fine-tune the publicly released pre-trained model on our AVW-4k dataset.
- **AudioLDM** [30] is a latent diffusion model for audio generation, capable of producing high-fidelity audio conditioned on either text or reference audio. It has been widely applied to tasks such as audio inpainting, style transfer, and super-resolution. To adopt it as an audio-only baseline for comparison with world models, we encoded the action vectors via an MLP and integrated them into AudioLDM’s original audio conditioning features, allowing the model to generate future audio frames from context audio frames under precise action supervision. We fine-tuned a pre-trained AudioLDM model on the AVW-4k dataset to compare with our work.

Results. As shown in Table 3, our AVWM outperforms modality-factorized baselines across most visual and auditory metrics. In specific cases, it maintains highly competitive performance. While unimodal models excel within their respective domains, our framework achieves superior fidelity by capturing the intrinsic physical links between sight and sound.

Table 4: Performance under **fixed-step** generation mode during training stages. We report the mean and standard deviation for each metric calculated over three runs. ‘∅’ marks that the model does not produce outputs for this modality at this stage.

Training stages	Vision				Audio			Reward
	LPIPS↓	DreamSim↓	PSNR↑	FID↓	LSD↓	SSIM↑	FAD↓	MSE↓
Pretrained NWM	0.628 ± 0.000	0.516 ± 0.000	11.828 ± 0.001	89.412 ± 0.058	∅	∅	∅	∅
Training Stage 1	0.382 ± 0.000	0.258 ± 0.000	16.539 ± 0.001	25.906 ± 0.034	∅	∅	∅	∅
Training Stage 1+2	∅	∅	∅	∅	1.297 ± 0.000	0.531 ± 0.000	2.684 ± 0.001	0.889 ± 0.006
Training Stage 1+2+3 (ours)	0.382 ± 0.000	0.255 ± 0.000	16.504 ± 0.005	24.347 ± 0.023	1.311 ± 0.000	0.547 ± 0.000	2.391 ± 0.001	0.746 ± 0.002

Table 5: Performance under **rollout** generation mode during training stages. Other settings are the same as the Table 4.

Training stages	Vision				Audio			Reward
	LPIPS↓	DreamSim↓	PSNR↑	FID↓	LSD↓	SSIM↑	FAD↓	MSE↓
Pretrained NWM	0.667 ± 0.000	0.557 ± 0.000	11.435 ± 0.008	87.335 ± 0.097	0	0	0	0
Training Stage 1	0.414 ± 0.000	0.278 ± 0.000	15.941 ± 0.005	26.227 ± 0.032	0	0	0	0
Training Stage 1+2	0	0	0	0	1.628 ± 0.000	0.544 ± 0.000	1.645 ± 0.004	0.062 ± 0.000
Training Stage 1+2+3 (ours)	0.407 ± 0.000	0.272 ± 0.000	16.019 ± 0.006	23.871 ± 0.073	1.620 ± 0.000	0.577 ± 0.000	1.315 ± 0.002	0.052 ± 0.000

5.3 Performance Evolution during Training Stages

Setup. We report the generative performance across the complete training stages, including a pre-trained NWM without training on AVW-4k, AV-CDiT fine-tuned on images (after stage 1), on audio (after stage 2), and jointly on both modalities (after stage 3). Furthermore, to evaluate the model’s capacity for spatial reasoning, we require it to predict a pseudo-reward: the reduction in shortest-path distance to the sound source between consecutive steps.

For each experimental configuration, we perform prediction and evaluation under two generation modes. In the **fixed-step** generation mode, given a specified temporal offset Δt , the model directly predicts the outcome at frame $t + \Delta t$. We iterate Δt over a 16-frame horizon ahead of the current frame. In the **rollout** generation mode, the model performs autoregressive prediction, where each generated frame is recursively used as input to produce the subsequent frame until reaching frame $t + 16$. Notably, reward magnitudes in fixed-step mode are inherently larger than in rollout mode, as the displacement between non-adjacent frames typically exceeds that of consecutive steps.

Results. As shown in Tables 4 and 5, the three-stage training strategy effectively enables the model to maintain strong generative performance across both visual and auditory modalities.

After the first stage, the model’s visual generation quality improves substantially. After the second stage, the model develops the ability to reasoning on auditory modality and generate plausible auditory outputs. After the third stage, the model not only retains the modality-specific knowledge learned in the previous stages-thus avoiding catastrophic forgetting-but also achieves better cross-modal alignment and joint representation learning, leading to further improvements in generation quality, particularly in the auditory modality.

Beyond these settings, we further investigated the effect of unfreezing all layers across all stages. This led to divergence in the second stage despite extensive hyperparameter tuning, which demonstrates that maintaining fixed attention in the second stage is vital to preserve pre-trained spatial knowledge and prevent catastrophic forgetting.

Table 6: Ablation under **fixed-step** generation mode. We report the mean and standard deviation for each metric calculated over three runs.

Ablation	Vision				Audio			Reward
	LPIPS↓	DreamSim↓	PSNR↑	FID↓	LSD↓	SSIM↑	FAD↓	MSE↓
w/o modality experts	0.378 ± 0.000	0.253 ± 0.000	16.536 ± 0.002	24.342 ± 0.011	1.366 ± 0.000	0.485 ± 0.000	2.772 ± 0.001	1.357 ± 0.008
w/o stagewise training	0.380 ± 0.000	0.253 ± 0.000	16.545 ± 0.002	24.466 ± 0.007	1.371 ± 0.000	0.485 ± 0.000	2.758 ± 0.001	1.294 ± 0.006
AV-CDiT (ours)	0.382 ± 0.000	0.255 ± 0.000	16.504 ± 0.005	24.347 ± 0.023	1.311 ± 0.000	0.547 ± 0.000	2.391 ± 0.001	0.746 ± 0.002

Table 7: Ablation under **rollout** generation mode. Other settings are the same as the Table 6.

Ablation	Vision				Audio			Reward
	LPIPS↓	DreamSim↓	PSNR↑	FID↓	LSD↓	SSIM↑	FAD↓	MSE↓
w/o modality experts	0.403 ± 0.000	0.270 ± 0.000	16.013 ± 0.001	23.860 ± 0.072	1.668 ± 0.000	0.515 ± 0.000	2.007 ± 0.003	0.038 ± 0.000
w/o stagewise training	0.404 ± 0.000	0.269 ± 0.000	16.089 ± 0.004	24.180 ± 0.051	1.614 ± 0.000	0.507 ± 0.000	2.007 ± 0.007	0.040 ± 0.000
AV-CDiT (ours)	0.407 ± 0.000	0.272 ± 0.000	16.019 ± 0.006	23.871 ± 0.073	1.620 ± 0.000	0.577 ± 0.000	1.315 ± 0.002	0.052 ± 0.000

5.4 Ablations

Setup. We conduct ablation studies to verify the effects of the modality experts and the stagewise training strategy. Specifically, we report the generative performance under two ablated settings. In the first setting, the modality experts are removed and replaced with a shared feed-forward network, where the audio and visual token sequences are jointly processed. In the second setting, the modality experts are retained, but the model is directly fine-tuned on both modalities simultaneously. As in Section 5.3, we report results under both generation modes.

Results. As shown in Tables 6 and 7, after introducing modality experts and applying the stagewise training strategy, AV-CDiT maintains comparable generative performance in the visual modality, while exhibiting a remarkable improvement in the auditory modality. This result further validates our hypothesis that *both modality experts and stagewise training helps preserve the model’s visual generation capability while preventing the dominant visual representations from overwhelming the auditory branch*. In other words, this strategy effectively mitigates modality imbalance and enables the model to better learn and generate audio signals in a coordinated manner.

Figure 5 presents qualitative comparisons among AV-CDiT and its ablated variants under both generation modes, while Figure 6 illustrates the temporal evolution of audio and reward prediction metrics across time steps under step-fixed generation mode, highlighting consistent improvements of AV-CDiT over the ablated models.

5.5 Planning with an Audio-Visual World Model

Setup. We evaluate the planning capability of AV-CDiT on the continuous audio-visual navigation (continuous AV-Nav) [9] task, where an agent navigates in a continuous 3D environment with egocentric RGB observations and binaural audio streams, and an episode is deemed successful if the agent issues a *stop* action within 1m of the target sound source.

The dataset of continuous AV-Nav is constructed on the SoundSpaces 2.0 simulation platform and the Matterport3D scenes, sharing the same action space as AVW-4k. The per-step reward consists of a success bonus, a constant negative step penalty, and the reduction in the shortest-path distance to the sound source, which aligns with the reward formulation used in AVW-4k. Therefore, the AVWM pretrained on AVW-4k can be directly applied to the continuous AV-Nav task without additional fine-tuning.

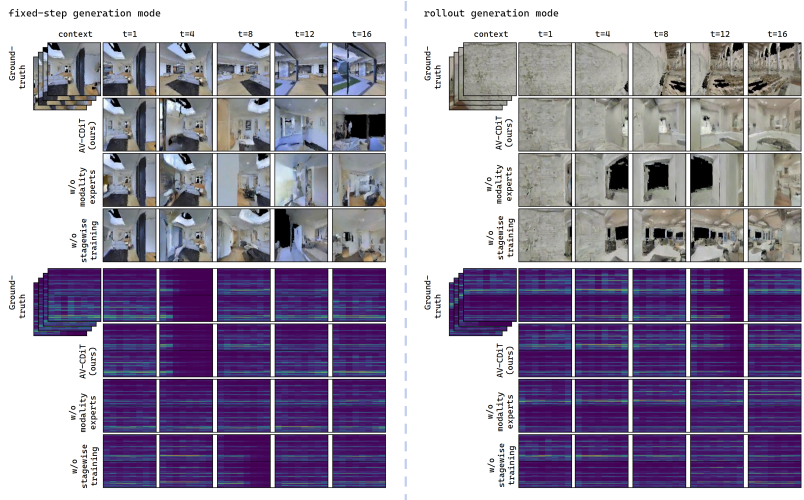


Fig. 5: Qualitative analysis. **Left** and **right** respectively show image and audio generation results of our model and two ablated variants under the fixed-step and rollout modes.

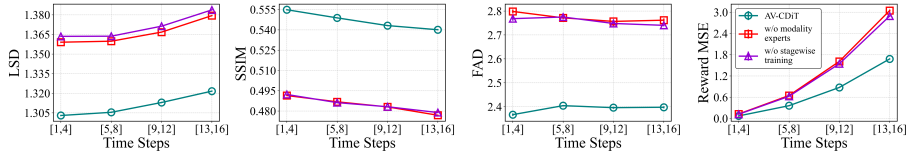


Fig. 6: Temporal evolution of audio generation quality and reward prediction in step-fixed mode. The curves show the averaged performance of AV-CDiT and ablated variants over four future time-step intervals.

Specifically, we employ the following algorithm to enhance a pretrained baseline AV-Nav agent [9] using a trained AVWM.

At each environment timestep t , instead of sampling only one action from the current policy, the agent samples n candidate actions from its policy distribution. Each candidate action is then propagated through the world model for a k -step audio-visual rollout, producing predicted observations and rewards for the future sequence. At each rollout step, the predicted immediate reward from AVWM is combined with the policy network’s value estimation, discounted over time, to compute the cumulative branch score. A beam search procedure is performed across rollout steps to retain up to B top-scoring action sequences. After the lookahead process is completed for the current timestep, the sequence with the highest cumulative score is selected, and its first action is executed in the real environment.

We report navigation performance under different beam widths B and rollout lengths k with the number of candidate actions to $n = 2$. The performance is evaluated using these common navigation metrics: success weighted by path

Table 8: Performance improvement of the continuous AV-Nav agent with the integration of AVWM. ‘Oracle WM’ denotes an upper bound obtained by replacing the imagined audio-visual outcomes and predicted task reward from AVWM with the ground-truth environment feedback. Except for NA, all metrics are in percentages, and statistical significance is validated via t-tests ($p < 0.05$).

		SPL↑	SoftSPL ↑	NA↓	SNA ↑	
AV-Nav Agent		45.08	55.09	332.817	6.44	
$B = 3$	$k = 4$	AVWM	45.70	56.54	321.11	6.67
		Oracle WM	51.02	60.71	300.35	8.36
	$k = 5$	AVWM	47.38	56.53	317.19	7.09
		Oracle WM	51.98	61.44	297.68	8.53
$B = 4$	$k = 4$	AVWM	46.46	57.00	317.99	6.87
		Oracle WM	51.64	60.58	298.25	8.48
	$k = 5$	AVWM	46.74	57.24	317.82	6.84
		Oracle WM	50.50	60.58	301.52	8.17

length (SPL), softSPL, number of actions (NA), and success normalized by action (SNA).

Results. As shown in Table 8, incorporating AVWM into the planning process effectively enhances the agent’s navigation performance under proper parameter configurations. In particular, the improvement in navigation efficiency, reflected by a significant reduction in the number of actions (NA), is especially pronounced. This is because AVWM enables the agent to evaluate multiple possible future outcomes before acting, leading to more informed and goal-directed decisions that reduce unnecessary exploration and shorten trajectories. Figure 7 illustrates a comparison of navigation trajectories under different settings.

6 Conclusion and Future Work

In this paper, we introduce AVWM, a framework for synchronized audio-visual simulation, supported by our fine-grained AVW-4k dataset and realized through the AV-CDiT architecture.

Currently, AV-CDiT has been trained and evaluated only on synthetic datasets such as AVW-4k. This is primarily due to the absence of real-world datasets that provide both precise action labels and highly synchronized audio-visual streams (refer to Section 3.3 for a detailed discussion of related datasets). In the future, larger-scale and more complex real-world datasets could be developed to further evaluate AVWM’s performance and robustness in more diverse and unpredictable environments. Furthermore, the modality-expert architecture and stagewise training strategy employed by AV-CDiT are generic design principles. We anticipate that these strategies will remain effective and generalizable across a broader range of transformer-based generative backbones.



Fig. 7: Comparison of navigation trajectories produced by three agents: the baseline AV-Nav agent (green), the AV-Nav agent enhanced with AVWM planning (red; $n = 2$, $B = 3$, $k = 5$), and the upper-bound AV-Nav agent augmented with an oracle world model (blue).

References

1. Agarwal, N., Ali, A., Bala, M., Balaji, Y., Barker, E., Cai, T., Chattopadhyay, P., Chen, Y., Cui, Y., Ding, Y., et al.: Cosmos world foundation model platform for physical ai. arXiv preprint arXiv:2501.03575 (2025)
2. Alonso, E., Jelley, A., Micheli, V., Kanervisto, A., Storkey, A., Pearce, T., Fleuret, F.: Diffusion for world modeling: Visual details matter in atari. In: Thirty-eighth Conference on Neural Information Processing Systems (NeurIPS) (2024)
3. Bao, H., Wang, W., Dong, L., Liu, Q., Mohammed, O.K., Aggarwal, K., Som, S., Piao, S., Wei, F.: Vlm0: Unified vision-language pre-training with mixture-of-modality-experts. *Advances in neural information processing systems* **35**, 32897–32912 (2022)
4. Bar, A., Zhou, G., Tran, D., Darrell, T., LeCun, Y.: Navigation world models. In: Proceedings of the Computer Vision and Pattern Recognition Conference. pp. 15791–15801 (2025)
5. Blattmann, A., Dockhorn, T., Kulal, S., Mendeleevitch, D., Kilian, M., Lorenz, D., Levi, Y., English, Z., Voleti, V., Letts, A., et al.: Stable video diffusion: Scaling latent video diffusion models to large datasets. arXiv preprint arXiv:2311.15127 (2023)
6. Bruce, J., Dennis, M.D., Edwards, A., Parker-Holder, J., Shi, Y., Hughes, E., Lai, M., Mavalankar, A., Steigerwald, R., Apps, C., Aytar, Y., Bechtle, S., Behbahani, F., Chan, S., Heess, N., Gonzalez, L., Osindero, S., Ozair, S., Reed, S., Zhang, J., Zolna, K., Clune, J., de Freitas, N., Singh, S., Rocktäschel, T.: Genie: Generative interactive environments. In: Forty-first International Conference on Machine Learning (ICML) (2024)
7. Chang, A., Dai, A., Funkhouser, T., Halber, M., Niessner, M., Savva, M., Song, S., Zeng, A., Zhang, Y.: Matterport3d: Learning from rgb-d data in indoor environments. arXiv preprint arXiv:1709.06158 (2017)
8. Chen, C., Peng, P., Baid, A., Xue, Z., Hsu, W.N., Harwath, D., Grauman, K.: Action2sound: Ambient-aware generation of action sounds from egocentric videos. In: European Conference on Computer Vision. pp. 277–295. Springer (2024)
9. Chen, C., Schissler, C., Garg, S., Kobernik, P., Clegg, A., Calamia, P., Batra, D., Robinson, P., Grauman, K.: Soundspaces 2.0: A simulation platform for visual-acoustic learning. *Advances in Neural Information Processing Systems* **35**, 8896–8911 (2022)
10. Damen, D., Doughty, H., Farinella, G.M., Fidler, S., Furnari, A., Kazakos, E., Moltisanti, D., Munro, J., Perrett, T., Price, W., et al.: The epic-kitchens dataset: Collection, challenges and baselines. *IEEE Transactions on Pattern Analysis and Machine Intelligence* **43**(11), 4125–4141 (2020)
11. Dasari, S., Ebert, F., Tian, S., Nair, S., Bucher, B., Schmeckpeper, K., Singh, S., Levine, S., Finn, C.: Robonet: Large-scale multi-robot learning. arXiv preprint arXiv:1910.11215 (2019)
12. Ding, J., Zhang, Y., Shang, Y., Zhang, Y., Zong, Z., Feng, J., Yuan, Y., Su, H., Li, N., Sukiennik, N., et al.: Understanding world or predicting future? a comprehensive survey of world models. *ACM Computing Surveys* **58**(3), 1–38 (2025)
13. Du, H., Li, G., Zhou, C., Zhang, C., Zhao, A., Hu, D.: Crab: A unified audio-visual scene understanding model with explicit cooperation. In: Proceedings of the Computer Vision and Pattern Recognition Conference. pp. 18804–18814 (2025)
14. Erell, A., Weintraub, M.: Estimation using log-spectral-distance criterion for noise-robust speech recognition. In: International Conference on Acoustics, Speech, and Signal Processing. pp. 853–856. IEEE (1990)

15. Fu, S., Tamir, N., Sundaram, S., Chai, L., Zhang, R., Dekel, T., Isola, P.: Dreamsims: Learning new dimensions of human visual similarity using synthetic data. arXiv preprint arXiv:2306.09344 (2023)
16. Ge, Z., Huang, H., Zhou, M., Li, J., Wang, G., Tang, S., Zhuang, Y.: Worldgpt: Empowering llm as multimodal world model. In: Proceedings of the 32nd ACM International Conference on Multimedia. pp. 7346–7355 (2024)
17. Gemmeke, J.F., Ellis, D.P., Freedman, D., Jansen, A., Lawrence, W., Moore, R.C., Plakal, M., Ritter, M.: Audio set: An ontology and human-labeled dataset for audio events. In: 2017 IEEE international conference on acoustics, speech and signal processing (ICASSP). pp. 776–780. IEEE (2017)
18. Grauman, K., Westbury, A., Byrne, E., Chavis, Z., Furnari, A., Girdhar, R., Hamburger, J., Jiang, H., Liu, M., Liu, X., et al.: Ego4d: Around the world in 3,000 hours of egocentric video. In: Proceedings of the IEEE/CVF conference on computer vision and pattern recognition. pp. 18995–19012 (2022)
19. Guo, J., Ye, Y., He, T., Wu, H., Jiang, Y., Pearce, T., Bian, J.: Mineworld: a real-time and open-source interactive world model on minecraft. arXiv preprint arXiv:2504.08388 (2025)
20. Guss, W.H., Houghton, B., Topin, N., Wang, P., Codel, C., Veloso, M., Salakhutdinov, R.: Minerl: A large-scale dataset of minecraft demonstrations. arXiv preprint arXiv:1907.13440 (2019)
21. Hafner, D., Pasukonis, J., Ba, J., Lillicrap, T.: Mastering diverse control tasks through world models. Nature pp. 1–7 (2025)
22. He, Y., Weilbach, C.D., Wojciechowska, M.E., Zhang, Y., Wood, F.: Plaicraft: Large-scale time-aligned vision-speech-action dataset for embodied ai. arXiv preprint arXiv:2505.12707 (2025)
23. Heusel, M., Ramsauer, H., Unterthiner, T., Nessler, B., Hochreiter, S.: Gans trained by a two time-scale update rule converge to a local nash equilibrium. Advances in neural information processing systems **30** (2017)
24. Ho, J., Jain, A., Abbeel, P.: Denoising diffusion probabilistic models. Advances in neural information processing systems **33**, 6840–6851 (2020)
25. Karnan, H., Nair, A., Xiao, X., Warnell, G., Pirk, S., Toshev, A., Hart, J., Biswas, J., Stone, P.: Socially compliant navigation dataset (scand): A large-scale dataset of demonstrations for social navigation. IEEE Robotics and Automation Letters **7**(4), 11807–11814 (2022)
26. Kilgour, K., Zuluaga, M., Roblek, D., Sharifi, M.: Fréchet audio distance: A metric for evaluating music enhancement algorithms. arXiv preprint arXiv:1812.08466 (2018)
27. Kim, G., Martinez, A., Su, Y.C., Jou, B., Lezama, J., Gupta, A., Yu, L., Jiang, L., Jansen, A., Walker, J., et al.: A versatile diffusion transformer with mixture of noise levels for audiovisual generation. Advances in Neural Information Processing Systems **37**, 11837–11865 (2024)
28. Lee, S.H., Oh, G., Byeon, W., Kim, C., Ryoo, W.J., Yoon, S.H., Cho, H., Bae, J., Kim, J., Kim, S.: Sound-guided semantic video generation. In: European Conference on Computer Vision. pp. 34–50. Springer (2022)
29. Li, C., Chen, Z., Wang, L., Zhu, J.: Audio super-resolution with latent bridge models. arXiv preprint arXiv:2509.17609 (2025)
30. Liu, H., Chen, Z., Yuan, Y., Mei, X., Liu, X., Mandic, D., Wang, W., Plumbley, M.D.: Audioldm: Text-to-audio generation with latent diffusion models. arXiv preprint arXiv:2301.12503 (2023)

31. Liu, H., Kong, Q., Tian, Q., Zhao, Y., Wang, D., Huang, C., Wang, Y.: Voicefixer: Toward general speech restoration with neural vocoder. arXiv preprint arXiv:2109.13731 (2021)
32. Nichol, A.Q., Dhariwal, P.: Improved denoising diffusion probabilistic models. In: International conference on machine learning. pp. 8162–8171. PMLR (2021)
33. Pearce, T., Zhu, J.: Counter-strike deathmatch with large-scale behavioural cloning. In: 2022 IEEE Conference on Games (CoG). pp. 104–111. IEEE (2022)
34. Peebles, W., Xie, S.: Scalable diffusion models with transformers. In: Proceedings of the IEEE/CVF international conference on computer vision. pp. 4195–4205 (2023)
35. Rombach, R., Blattmann, A., Lorenz, D., Esser, P., Ommer, B.: High-resolution image synthesis with latent diffusion models. In: Proceedings of the IEEE/CVF conference on computer vision and pattern recognition. pp. 10684–10695 (2022)
36. Ronneberger, O., Fischer, P., Brox, T.: U-net: Convolutional networks for biomedical image segmentation. In: International Conference on Medical image computing and computer-assisted intervention. pp. 234–241. Springer (2015)
37. Ruan, L., Ma, Y., Yang, H., He, H., Liu, B., Fu, J., Yuan, N.J., Jin, Q., Guo, B.: Mm-diffusion: Learning multi-modal diffusion models for joint audio and video generation. In: Proceedings of the IEEE/CVF Conference on Computer Vision and Pattern Recognition. pp. 10219–10228 (2023)
38. Ryu, H., Kim, S., Chung, J.S., Senocak, A.: Seeing speech and sound: Distinguishing and locating audios in visual scenes. arXiv preprint arXiv:2503.18880 (2025)
39. Sung-Bin, K., Senocak, A., Ha, H., Owens, A., Oh, T.H.: Sound to visual scene generation by audio-to-visual latent alignment. In: Proceedings of the IEEE/CVF Conference on Computer Vision and Pattern Recognition. pp. 6430–6440 (2023)
40. Wang, Z., Bovik, A.C., Sheikh, H.R., Simoncelli, E.P.: Image quality assessment: from error visibility to structural similarity. IEEE transactions on image processing **13**(4), 600–612 (2004)
41. Wu, C., Chen, X., Wu, Z., Ma, Y., Liu, X., Pan, Z., Liu, W., Xie, Z., Yu, X., Ruan, C., et al.: Janus: Decoupling visual encoding for unified multimodal understanding and generation. In: Proceedings of the Computer Vision and Pattern Recognition Conference. pp. 12966–12977 (2025)
42. Wu, J., Yin, S., Feng, N., He, X., Li, D., Hao, J., Long, M.: ivideoopt: Interactive videoopts are scalable world models. Advances in Neural Information Processing Systems **37**, 68082–68119 (2024)
43. Wu, J., Yin, S., Feng, N., Long, M.: Rlvr-world: Training world models with reinforcement learning. arXiv preprint arXiv:2505.13934 (2025)
44. Wu, J., Zhang, X., Yuan, H., Zhang, X., Huang, T., He, C., Deng, C., Zhang, R., Wu, Y., Long, M.: Visual generation unlocks human-like reasoning through multimodal world models. arXiv preprint arXiv:2601.19834 (2026)
45. Xing, Y., He, Y., Tian, Z., Wang, X., Chen, Q.: Seeing and hearing: Open-domain visual-audio generation with diffusion latent aligners. In: Proceedings of the IEEE/CVF Conference on Computer Vision and Pattern Recognition. pp. 7151–7161 (2024)
46. Xu, J., Sun, X., Zhang, Z., Zhao, G., Lin, J.: Understanding and improving layer normalization. Advances in neural information processing systems **32** (2019)
47. Yu, T., Quillen, D., He, Z., Julian, R., Hausman, K., Finn, C., Levine, S.: Meta-world: A benchmark and evaluation for multi-task and meta reinforcement learning. In: Conference on robot learning. pp. 1094–1100. PMLR (2020)
48. Zeghidour, N., Luebs, A., Omran, A., Skoglund, J., Tagliasacchi, M.: Soundstream: An end-to-end neural audio codec. IEEE/ACM Transactions on Audio, Speech, and Language Processing **30**, 495–507 (2021)

49. Zhang, P.F., Cheng, Y., Sun, X., Wang, S., Zhu, L., Shen, H.T.: A step toward world models: A survey on robotic manipulation. arXiv preprint arXiv:2511.02097 (2025)
50. Zhang, R., Isola, P., Efros, A.A., Shechtman, E., Wang, O.: The unreasonable effectiveness of deep features as a perceptual metric. In: Proceedings of the IEEE conference on computer vision and pattern recognition. pp. 586–595 (2018)
51. Zhao, G., Wang, X., Zhu, Z., Chen, X., Huang, G., Bao, X., Wang, X.: Drivedreamer-2: Llm-enhanced world models for diverse driving video generation. In: Proceedings of the AAAI Conference on Artificial Intelligence. vol. 39, pp. 10412–10420 (2025)
52. Zhao, X., Wang, Y., Jin, P.: Audio-visual adaptive fusion network for question answering based on contrastive learning. In: Proceedings of the AAAI Conference on Artificial Intelligence. vol. 39, pp. 10483–10491 (2025)
53. Zhao, Z., Tang, H., Yan, Y.: Audio-visual navigation with anti-backtracking. In: International Conference on Pattern Recognition. pp. 358–372. Springer (2025)
54. Zuo, S., Zheng, W., Huang, Y., Zhou, J., Lu, J.: Gaussianworld: Gaussian world model for streaming 3d occupancy prediction. In: Proceedings of the Computer Vision and Pattern Recognition Conference. pp. 6772–6781 (2025)